NANO LETTERS

2008
Vol. 8, No. 1
152−156

Microwave Impedance Spectroscopy of Dense Carbon Nanotube Bundles

Alexander Tselev, Michael Woodson, Cheng Qian, and Jie Liu*

Chemistry Department, Duke University, Durham, North Carolina 27708

Received September 10, 2007; Revised Manuscript Received November 12, 2007

ABSTRACT

We have performed impedance spectroscopy of dense carbon nanotube (CNT) bundles in the broad frequency range from 10 MHz to 67 GHz. Dense CNT bundles were formed on sharp tips from aqueous suspension by ac dielectrophoresis and incorporated into on-wafer test structures. The frequency response of the bundles can be fit to a model with frequency-independent elements in the entire frequency range up to 67 GHz strongly suggesting that CNT properties do not depend on the frequency throughout the whole frequency range. The measurements at microwave frequencies allowed separate characterization of the bundle/metal electrode contacts and the bundle bulk. Effects of different CNT fabrication and suspension processing routes on bundle characteristics were identified. We have also made a preliminary estimation of the average inductance per current carrying shell in the bundles. For good quality nanotube bundles, the inductance has been found to fall within the range from approximately 3.5 to 40 nH/μm. With decreasing nanotube quality, the implemented estimation procedure yields higher values with a large uncertainty. Systematic measurements of devices with individual nanotubes are required to provide more accurate data.

Theoretical analysis shows that dense bundles of tens and hundreds of carbon nanotubes (CNT) may become an advantageous alternative to metal interconnects in future high-speed and ultrahigh-density electronic circuits because of their high current carrying capacity, stability against electromigration, and potentially better signal transmission performance associated with lower electrical resistance.[1−4] The realization of CNT interconnects constitutes a complex, challenging task for both development of suitable material and assembly techniques. While certain progress has been achieved so far in fabricating carbon nanotube vias,[5−8] currently there is no process allowing fabrication of CNT wires. We note that all published processes for fabrications of vias are based on the growth of carbon nanotubes directly on the wafer. However, a technique with CNT synthesis and processing removed from the wafer would provide much more freedom and flexibility for both development of the CNT material and for design of the circuit fabrication processes.

In this work, using an approach able to yield virtually 100% dense bundles of carbon nanotubes, we fabricate simple devices and perform impedance spectroscopy of top-contacted CNT bundles at microwave frequencies up to 67 GHz. Impedance spectroscopy allows the separation of contributions to device impedance from the metal/CNT contacts and those from the bundle bulk, which in turn allows characterization of the bundle material properties and the electrical parameters of the contacts. Because of the small contact capacitance (on the order of femtofarads) microwave frequencies (up to tens of gigahertz) are needed for meaningful spectroscopy.

Large impedance and small size make the characterization of CNT electrical properties at microwave frequencies a challenging task. "Bulky" (compared to the nanotubes) microwave electrical probes require test structures whose relatively large parasitics mask the CNT response. A large impedance mismatch with the measurement equipment dramatically degrades the measurement resolution. Informative experimental data on electrical properties of CNTs at gigahertz frequencies are rather sparse. Significant effort was spent to demonstrate the transistor action of CNTs at gigahertz frequencies.[8−13] Less work has been done toward testing CNT performance as wires.[14−18]

A large step forward was made by Plombon et al.,[19] who have performed electrical measurements of isolated single-walled CNTs (SWNT) up to 20 GHz with the goal of determining their kinetic inductance, which strongly dominates its magnetic counterpart and is one of the main factors limiting the theoretical maximum performance of CNT interconnects with respect to the signal propagation speed. A de-embedding technique was used to find the impedance of the nanotube contacted by electrodes. The properties of the SWNT were found by fitting the obtained frequency dependence of the impedance to the response of an equivalent circuit model. These measurements yielded a value of kinetic inductance of 39 nH/μm for an individual SWNT, which is almost 1 order of magnitude higher than the theoretical value of 4 nH/μm (see, e.g., ref 20). In this work, we have also made an attempt to determine the kinetic inductance of CNTs. However, large uncertainties associated with the

* Corresponding author. E-mail: j.liu@duke.edu.

10.1021/nl072315j CCC: $40.75
Published on Web 12/11/2007

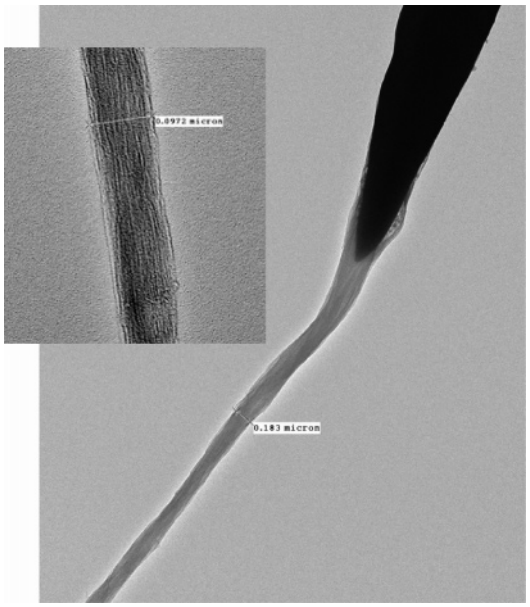

Figure 1. A dense CNT bundle attached to an indium tip. The bundle diameter at the white mark is 180 nm. Inset: A part of the bundle away from the root at higher magnification. The bundle diameter in the inset is 100 nm.

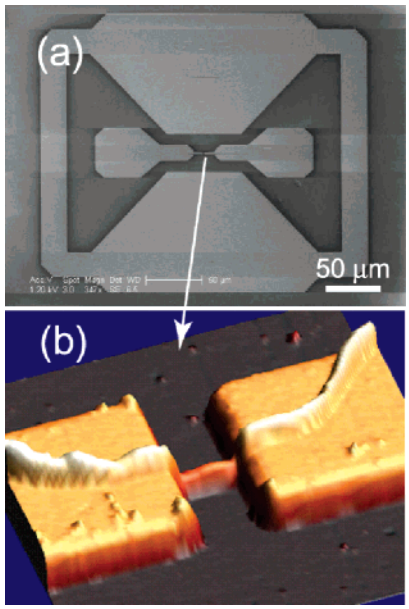

Figure 2. (a) SEM image of the test structure used for the measurements. (b) Atomic force microscopy (AFM) image of a bundle in the gap between signal electrodes of the test structure.[29] The gap width is 1 μm; the electrode width is 2 μm.

nature of the investigated material precluded us from providing a definite value, and consequently, only estimations of the inductance value have been performed.

We start with a review of our experimental techniques. Dense CNT bundles were assembled from aqueous suspensions onto sharp metal tips by ac dielectrophoresis (DEP).[21] Suspended CNTs are aligned and attracted to the tip by the gradient of an ac electric field (10 MHz frequency) between the tip and a counterelectrode. As the tip is gradually pulled out of the suspension, surface tension of the liquid compresses the nanotubes into a dense bundle. Transmission electron microscopy (TEM) investigation of the structure of the bundles shows good nanotube alignment and packing density (Figure 1).

Few-walled nanotubes (FWNTs) with an average diameter of about 5 nm were used in the experiments (which is not optimal for the interconnect application, but sufficient for the purpose of the present work). The tubes were synthesized by chemical vapor deposition in a relatively large-scale process, following a previously published procedure.[22] The FWNTs were treated with an oxidizing agent such as potassium permanganate ($KMnO_4$) or nitric acid (HNO_3) to provide sidewall functionalization with hydrophilic carboxylic acid groups. The nanotubes could then be easily dispersed in water by sonication to form relatively stable suspensions. Two differently prepared nanotube suspensions were used. Details of the suspension preparation can be found in Supporting Information.

The sharp metal tips were formed by withdrawing tungsten wire from an indium melt. Prior to bundle assembly, a film of gallium metal was evaporated onto the liquid nitrogen-cooled tips. The Ga film facilitated the bundle release onto the substrate for the following device fabrication. Tip-mounted bundles were aligned with lithographically printed alignment marks and laid down on a quartz substrate by micromanipulators. The substrate was heated to about 80 °C to melt the Ga film on the tip (Ga melting point is 30 °C) and release the attached bundle. The exact location of the bundle relative to the alignment marks was then determined by scanning electron microscopy (SEM), and the test structure (Figure 2) was fabricated in a two-step process. First, electron beam lithography was used to pattern electrical contacts to the bundles followed by e-beam evaporation of an 80 nm thick Pd layer with a 30 nm Au layer on top and lift-off. Second, the test structure was completed with fabrication of probe contact pads and test structure grounds by either conventional photolithography or e-beam lithography. Large contact pads and grounds were made of 130 nm thick Au layers with a 3 nm Cr layer underneath. Some of the bundles were annealed at 500 °C under flowing hydrogen for 20 min right before contact fabrication. The e-beam writing used a 9 nm thick aluminum film evaporated on top of the photoresist to prevent charging of the dielectric substrate.

Impedance spectroscopy of dense FWNT bundles was performed in the frequency range of 10 MHz to 67 GHz utilizing *S*-parameter measurements and a de-embedding technique. The *S*-parameters of the test structures were measured with a vector network analyzer (Agilent E8361A) and a microwave probe station (Cascade Microtech, Infinity GSG probes, 100 μm pitch). The measurements were made at the microwave power level of −5 dBm corresponding to a voltage drop across the contacted bundle of 350 mVp-p and the bundle being in the linear regime. The bundle impedance was de-embedded from the test structure parasitics characterized using dummy structures fabricated near the actual test structure.[23,24] The de-embedding procedure developed for these measurements is described in detail in the Supporting Information. To extract properties of the bundle

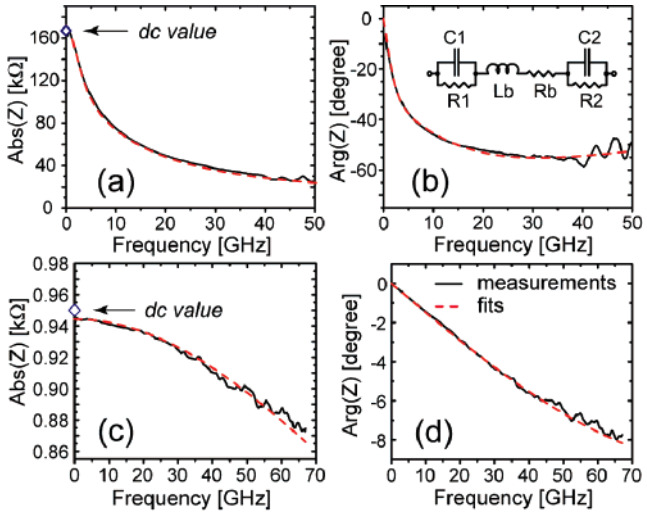

Figure 3. Solid lines are de-embedded impedance vs frequency curves for two representative bundles. Dashed lines are fits of the measured data to the response of the equivalent circuit model shown as an inset in panel b. Diamonds show resistance values obtained by dc measurements. (a,b) Absolute value and phase, respectively, of the impedance for bundle 2 (Table 1); (c,d) same for bundle 8.

and the contacts, the measured frequency dependence of the bundle impedance was fit to the equivalent lumped element model with frequency-independent elements. Figure 3 shows examples of the de-embedded impedance versus frequency curves with their fits for two bundles. Similar to ref 19, we used a model (Figure 3b, inset) in which contacts are represented by parallel RC pairs, and an inductor with a resistor in series represents the bulk of the bundle. However, we assume that properties of the two electrode-bundle contacts are different, which is supported by the results of ref 16. We note that different authors use different equivalent circuits for interpretation of high-frequency measurements, but the choice of the physical model of the system is crucial for meaningful impedance spectroscopy results. Because the kinetic inductance of the nanotubes is expected to be large, a series resistor−inductor pair should be included between contacts dominating the shape of the frequency response, especially, when the contact resistance is large.

As is seen from Figure 3, good fittings can be obtained throughout the entire frequency range up to 67 GHz with use of a fitting model with frequency-independent elements. This strongly suggests that the CNT properties are independent of the frequency up to at least 67 GHz.

CNT suspensions prepared by different methods yielded different solubility, nanotube length distributions, and cleanliness of the CNT surface, all of which influence the formation of bundles and their properties. Suspension 1 consisted of FWNTs with average length of about 0.4 μm, which is less than the length of the bundle portion between the signal electrodes of the test structure (approximately 1 μm). Treatment of nanotubes during the preparation of this suspension with an aggressive oxidizer resulted in more defects on the outer walls and led to partial coverage of the nanotubes with amorphous carbon. In contrast, the average length of the nanotubes in suspension 2 was close to 4 μm and tubes were partially bundled. The oxidizer used for this

Table 1. Bundle Diameters, D, and Values of Parameters for the Equivalent Circuit Model (Shown in the Inset of Figure 3b) Obtained for Ten CNT Bundles through the Fitting Procedure[a]

No.	D (nm)	R_b (kΩ)	L_b (nH)	R_1 (kΩ)	R_2 (kΩ)	C_1 (fF)	C_2 (fF)	L_t (nH/μm)
1	105	12.9	0.2	85.3	39.1	0.3	0.1	
2	75	10.7	0.3	109.9	51.3	0.5	0.2	
3	90	7.3	0.2	19.0	9.0	0.3	1.9	
4	190	0.8	1.1	1.9	1.2	1.0	1.4	
5	70	0.63	0.11	2.74	1.14	3.3	1.3	0.8
6	84	0.20	0.56	0.74	2.17	5.0	0.5	12.1
7	70	0.37	1.51	1.91	1.69	0.5	0.6	18.0
8	142	0.10	0.19	0.45	0.40	2.6	0.4	8.6
9	71	0.22	0.62	0.62	2.37	6.9	0.5	12.2
10	150	0.16	0.29	0.81	0.86	2.6	0.3	8.2

[a] The rightmost column shows estimated values of the inductance per current carrying shell. Bundles 1−4 were made from suspension 1, as described in the text. Bundles 5−10 were made from suspension 2. Bundles 4 and 8−10 were annealed at 500 °C under flowing hydrogen for 20 min prior to contact fabrication. Bundle diameters D were measured by AFM.

suspension does not produce any significant number of new defects in the FWNT outer walls.

Table 1 summarizes the results of the fittings for ten bundles made from these two suspensions. It is apparent that the bundles of suspension 1 are significantly less conductive than those of suspension 2. Generally, the properties of the two contacts to an individual bundle appear quite different. Annealing in hydrogen noticeably reduces the intrinsic and contact resistance of the bundles made from suspension 1, but still the resistance R_b of bundle 4 is larger that that of all bundles made from suspension 2. It can be explained by the fact that the intertube coupling in the bundle is weak,[25,26] and the tube−tube resistance is, consequently, large. The average length of nanotubes in bundle 4 is smaller than the gap width, which means that only a few nanotubes out of the hundreds physically present in the bundle are long enough to be contacted at both ends and are participating in the conduction. Because the average length of the CNTs in suspension 2 is much larger than the gap between the electrodes of the test structure, we can expect that a large fraction of the tubes will span the entire gap. There is no noticeable effect of annealing on the electrical conductance of the bundles of suspension 2. The annealing has no noticeable effect on the contact capacitance, either. On the basis of these considerations, we include only bundles made from suspension 2 in the further analysis.

Figure 4 displays the magnitude of the transmission signal S12 for the test structures with bundles 5 through 10 and the corresponding open structure responses. It is worth noting the behavior of the signal for bundle 5, which is outside the trend set by five other samples. Because the signals from open structures are highly reproducible, the "anomaly" cannot be attributed to variations of the test structure geometry. Presumably, it can be a result of a large isolated defect in the bundle structure, which was not detected by other techniques. For example, a defect may separate two parts of the bundle and decrease coupling between them at low frequencies. However, a significant capacitive coupling may

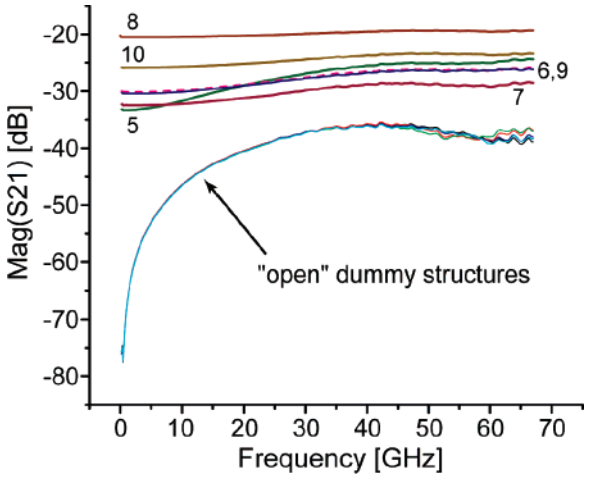

Figure 4. Magnitude of S21 (transmission) signals for the test structures with bundles 5 through 10 in Table 1 and for the corresponding open dummy structures.

exist between the parts separated by the defect, and it becomes noticeable through the relative increase of the magnitude of the S12 signal at higher frequencies.

Bundles 5−10 have been made from the same suspension, and it is reasonable to consider that the material quality and CNT diameter distribution are the same for all the bundles. Then, the measurement data can be further analyzed in terms of parameters common to all the bundles. The values of inductance are of particular interest, and in the following we will focus on them. Tentatively, we choose averaged values per current carrying shell to examine the data.

First, we make estimations of the number n of current-carrying shells in each bundle using the intrinsic bundle resistance R_b and intrinsic resistance per unit length ρ of a metallic single-walled CNT: $n = \rho l / R_b$, where l is the bundle length. As has been mentioned above, the tube−tube and shell−shell (for FWNTs) electrical coupling is weak, and we can ignore the current flowing between shells. The room-temperature value $\rho = 11$ kΩ/μm was found recently by Purewal et al.[27] for a 2 nm diameter high-quality metallic SWNT. The portion of the nanotube resistance due to acoustic phonons is inversely proportional to the tube diameter d: $\rho \sim 1/d$.[28] Assuming the average diameter of nanotubes in the bundles is equal to 5 nm, we take ρ (5 nm) $=$ 4.4 kΩ/μm for the outer shells of our FWNTs as a lower boundary value for the parameter ρ.

Next, we estimate the average kinetic inductance per current carrying shell using this value. Because the kinetic inductance scales linearly with the number of current carrying shells, the inductance per shell can be calculated as

$$L_t = nL_b = \rho L_b / R_b \qquad (1)$$

The last equality is valid taking into account that $l = 1$ μm for our bundles. The result of these calculations is shown in the rightmost column of Table 1. We note that the value of L_t for bundle 5 is significantly less than that for other bundles, which is apparently one of the consequences of the earlier discussed "anomaly" in response of this bundle. The values for bundles 6 and 8−10 are close to each other showing a good consistency of the measurement procedure. They group around 10 nH/μm, which is close to the theoretically predicted 4 nH/μm. However, measurement uncertainties must be taken into account for a correct interpretation of the data.

Uncertainty of the values of R_b and L_b obtained through the fitting procedure can be roughly estimated to be around 50%. The true value of the ratio L_b/R_b can then fall between values by a factor of $1.5^2 = 2.25$ smaller and, respectively, larger than those that follow from the data of Table 1. Taking this into account, the lower value for the averaged inductance per current carrying shell can be determined to be approximately 3.5 nH/μm based on $L_t = 8.2$ nH/μm for bundle 10. Analogously, the upper value can be calculated to be approximately 40 nH/μm based on $L_t = 18.0$ nH/μm for bundle 7. However, for lower quality tubes with a greater number of defects, the parameter ρ in eq 1 can be significantly larger than the value taken for the estimations assuming a good quality of the nanotubes in the bundles. Therefore, strictly speaking, the upper boundary for the inductance per shell cannot be definitively defined by this method. We can estimate that for our nanotubes, the value of ρ can be up to 2 times larger that that used to calculate values of L_t in Table 1. Combined with the uncertainties of R_b and L_b, it yields the upper value of about 55 nH/μm based on $L_t \approx 12.0$ nH/μm for bundles 6 and 9. Further, this issue can be resolved through systematic measurements of devices with individual high-quality single-walled nanotubes. Additionally, careful analysis of measurement errors associated with particular de-embedding procedures and limited measurement resolution should be performed. Experiments in these directions are currently in progress in our laboratory.

To summarize, we have performed broadband microwave-frequency impedance spectroscopy of top-contacted, dense CNT bundles consisting of a few hundred FWNTs. Importantly, the frequency response of the bundle can be fit to a model with frequency-independent elements in the whole frequency range up to 67 GHz, which indicates that the CNT properties are frequency-independent up to at least 67 GHz. Impedance spectroscopy allowed us to identify the effect of different procedures for CNT suspension preparation and annealing on resistance of the bundle bulk and on the contact resistance. Because of the nature of the investigated CNT material, the measurement uncertainties appear to be too large to obtain accurate quantitative information about properties of individual nanotubes forming the bundles. However, we made conservative estimates of the range where the kinetic inductance per current carrying shell may fall. For good quality nanotube bundles, the inductance has been found to be within the range between approximately 3.5 and 40 nH/μm. With decreasing nanotube quality, the estimation procedure yields higher values with a large uncertainty. Systematic measurements of devices with individual nanotubes are required to provide accurate values.

Acknowledgment. The authors greatly acknowledge financial support granted by the Arrowhead Research Corporation.

Supporting Information Available: Detailed description of the CNT bundle impedance de-embedding technique, the methods of FWNT suspension preparation, estimation of uncertainty of the extracted values of R_b and L_b, and additional estimates of the upper boundary for the value of the inductance per current carrying shell. This material is free of charge via the Internet at http://pubs.acs.org.

References

(1) Naeemi, A.; Meindl, J. D. *IEEE Trans. Electron Devices* **2007**, *54*, 26.
(2) Naeemi, A.; Meindl, J. D. *IEEE Electron Device Lett.* **2006**, *27*, 338.
(3) Nieuwoudt, A.; Massoud, Y. *IEEE Trans. Electron Devices* **2006**, *53*, 2460.
(4) Cho, H.; Koo, K.-H.; Kapur, P.; Saraswat, K. C. In *The Delay, Energy, and Bandwidth Comparisons between Copper, Carbon Nanotube, and Optical Interconnects for Local and Global Wiring Application*, Proceedings of IEEE 2007 International Interconnect Technology Conference, June 4−6, 2007; IEEE: Burlingame, CA, 2007; p 135.
(5) Awano, Y.; Sato, S.; Kondo, D.; Ohfuti, M.; Kawabata, A.; Nihei, M.; Yokoyama, N. *Phys. Status Solidi A* **2006**, *203*, 3611.
(6) Nihei, M.; Hyakushima, T.; Sato, S.; Nozue, T.; Norimatsu, M.; Mishima, M.; Murakami, T.; Kondo, D.; Kawabata, A.; Ohfuti, M.; Awano, Y. In *Electrical Properties of Carbon Nanotube Via Interconnects Fabricated by Novel Damascene Process*, Proceedings of IEEE 2007 International Interconnect Technology Conference, June 4−6, 2007; IEEE: Burlingame, CA, 2007; p 204.
(7) Xu, T.; Wang, Z.; Miao, J.; Chen, X.; Tan, C. M. *Appl. Phys. Lett.* **2007**, *91*, 042108.
(8) Rosenblatt, S.; Lin, H.; Sazonova, V.; Tiwari, S.; McEuen, P. L. *Appl. Phys. Lett.* **2005**, *87*, 153111.
(9) Li, S.; Yu, Z.; Yen, S. F.; Tang, W. C.; Burke, P. J. *Nano Lett.* **2004**, *4*, 753.
(10) Singh, D. V.; Jenkins, K. A.; Appenzeller, J.; Neumayer, D.; Grill, A.; Wong, H. S. P. *IEEE Trans. Nanotechnol.* **2004**, *3*, 383.
(11) Appenzeller, J.; Frank, D. J. *Appl. Phys. Lett.* **2004**, *84*, 1771.
(12) Pesetski, A. A.; Baumgardner, J. E.; Folk, E.; Przybysz, J. X.; Adam, J. D.; Zhang, H. *Appl. Phys. Lett.* **2006**, *88*, 113103.
(13) Louarn, A. L.; Kapche, F.; Bethoux, J. M.; Happy, H.; Dambrine, G.; Derycke, V.; Chenevier, P.; Izard, N.; Goffman, M. F.; Bourgoin, J. P. *Appl. Phys. Lett.* **2007**, *90*, 233108.
(14) Yu, Z.; Burke, P. J. *Nano Lett.* **2005**, *5*, 1403.
(15) Zhang, M.; Huo, X.; Chan, P. C. H.; Liang, Q.; Tang, Z. K. *Appl. Phys. Lett.* **2006**, *88*, 163109.
(16) Rice, P.; Wallis, T. M.; Russek, S. E.; Kabos, P. *Nano Lett.* **2007**, *7*, 1086.
(17) Gomez-Rojas, L.; Bhattacharyya, S.; Mendoza, E.; Cox, D. C.; Rosolen, J. M.; Silva, S. R. P. *Nano Lett.* **2007**, *7*, 2672.
(18) Jun, S. C.; Huang, X. M. H.; Moon, S.; Kim, H. J.; Hone, J.; Jin, Y. W.; Kim, J. M. *New J. Phys.* **2007**, *9*, 265.
(19) Plombon, J. J.; O'Brien, K. P.; Gstrein, F.; Dubin, V. M.; Jiao, Y. *Appl. Phys. Lett.* **2007**, *90*, 063106.
(20) Anantram, M. P.; Léonard, F. *Rep. Prog. Phys.* **2006**, *69*, 507.
(21) Tang, J.; Gao, B.; Geng, H.; Velev, O. D.; Qin, L. C.; Zhou, O. *Adv. Mater.* **2003**, *15*, 1352.
(22) Qi, H.; Qian, C.; Liu, J. *Chem. Mater.* **2006**, *18*, 5691.
(23) Cho, H.; Burk, D. E. *IEEE Trans. Electron Devices* **1991**, *38*, 1371.
(24) Kolding, T. E. *IEEE Trans. Electron Devices* **2000**, *47*, 734.
(25) Stahl, H.; Appenzeller, J.; Martel, R.; Avouris, P.; Lengeler, B. *Phys. Rev. Lett.* **2000**, *85*, 5186.
(26) Tunney, M. A.; Cooper, N. R. *Phys. Rev. B* **2006**, *74*, 075406.
(27) Purewal, M. S.; Hong, B. H.; Ravi, A.; Chandra, B.; Hone, J.; Kim, P. *Phys. Rev. Lett.* **2007**, *98*, 186808.
(28) Zhou, X.; Park, J.-Y.; Huang, S.; Liu, J.; McEuen, P. L. *Phys. Rev. Lett.* **2005**, *95*, 146805.
(29) To produce this image, the AFM data have been post-processed with the help of *WSxM*, version 2.2 software acquired free of charge from Nanotec Electronica S.L. http://www.nanotec.es (accessed June 1, 2007).

NL072315J